CHEMISTRY
A EUROPEAN JOURNAL

Oxidation States and CO Ligand Exchange Kinetics in a Self-Assembled Monolayer of a Triruthenium Cluster Studied by In Situ Infrared Spectroscopy

Wei Zhou,[a, b] Shen Ye,*[a, b] Masaaki Abe,[c] Takuma Nishida,[a, b] Kohei Uosaki,*[c] Masatoshi Osawa,[a, b] and Yoichi Sasaki*[c]

Abstract: Oxidation states and CO ligand exchange kinetics in a self-assembled monolayer (SAM) of an oxo-centered triruthenium cluster $[Ru_3(\mu_3\text{-}O)(\mu\text{-}CH_3COO)_6(CO)(L^1)(L^2)]$ (L^1 = $[(NC_5H_4)CH_2NHC(O)(CH_2)_{10}S\text{-}]_2$, L^2 = 4-methylpyridine) have been extensively investigated on the surface of a gold electrode in aqueous and nonaqueous solutions. The SAM exhibits three consecutive one-electron transfers and four oxidation states, which have been characterized by electrochemistry, in situ infrared spectroscopy, and in situ sum frequency generation (SFG) vibrational spectroscopy measurements. The original electron-localized state of the Ru cluster center was changed to electron delocalization states by oxidation or reduction of the central Ru ions. These changes are revealed by the IR absorptions of the CO ligand and the bridging acetate ligands of the triruthenium cluster in the SAM. The IR absorptions of the two kinds of ligands are strongly dependent on the oxidation state of the Ru cluster center. One-electron oxidation of the central Ru ion in the SAM triggers a CO ligand liberation process. Solvent molecules may then occupy the CO site to result in a CO-free SAM. One-electron reduction of this CO-free SAM in a CO-saturated solution leads to re-coordination of the CO ligand into the SAM. Both processes can be precisely controlled by tuning the electrode potential. The kinetics of the CO exchange cycle in the SAM, including liberation and coordination, has been investigated by in situ IR and SFG measurements for the first time. The CO exchange cycle is significantly dependent on the temperature. The reaction rate greatly decreases with decreasing solution temperature, which is an important factor in the CO ligand exchange process. The activation energies of both CO liberation and coordination have been evaluated from the reaction rate constants obtained at various temperatures.

Keywords: IR spectroscopy · kinetics · ligand exchange · ruthenium · self-assembled monolayers · surface chemistry

Introduction

Recent progress made in basic studies and in applications of molecular electronic devices has encouraged efforts in the construction of novel molecular materials into ordered functionalized nanostructures.[1–3] Self-assembled monolayers (SAMs) based on alkanethiols or dialkyl disulfides are suitable templates that can be employed to build molecular units into ordered functional layers on electrode surfaces.[4–7] Tailoring SAMs with functional groups (in general, $HS\text{-}(CH_2)_n\text{-}X$) provides unique opportunities to improve our fundamental understanding of these functional components and also offers novel functionalized structures that may allow new applications in the fields of molecular switches, sensors, nanoelectronics, and optical devices, etc.[4,8–11]

[a] W. Zhou, Prof. S. Ye, T. Nishida, Prof. M. Osawa
Catalysis Research Center, Hokkaido University
Sapporo 001–0021 (Japan)
Fax: (+81) 11-706-9126
E-mail: ye@cat.hokudai.ac.jp

[b] W. Zhou, Prof. S. Ye, T. Nishida, Prof. M. Osawa
Division of Material Science
Graduate School of Environmental Earth Science
Hokkaido University
Sapporo 060–0810 (Japan)

[c] Dr. M. Abe, Prof. K. Uosaki, Prof. Y. Sasaki
Division of Chemistry, Graduate School of Science
Hokkaido University
Sapporo 060–0810 (Japan)

Supporting information for this article is available on the WWW under http://www.chemeurj.org/ or from the author.

DOI: 10.1002/chem.200401340

Transition-metal complexes with versatile chemical and physical properties are attractive components employed in functionalized monolayer or multilayer construction.[12–16] Among them, the oxo-centered triruthenium cluster with the general formula $[Ru_3(\mu_3\text{-}O)(\mu\text{-}CH_3COO)_6L_3]^n$ (L is a monodentate terminal ligand; n = net charge) is a prominent candidate owing to its unique properties that include reversible multielectron transfer, site-selective terminal ligand substitution reactions in solution, ligand-bridged oligomeric structure formation, and catalysis.[17–28] Fabrication of the cluster into a monolayer or a multilayer will provide novel functional nanostructures and new related applications.

Recently, we succeeded in constructing a SAM containing an oxo-centered triruthenium cluster from the complex $[Ru_3(\mu_3\text{-}O)(\mu\text{-}CH_3COO)_6(CO)(L^1)(L^2)]^0$ (Scheme 1, L^1 = $[(NC_5H_4)CH_2NHC(O)(CH_2)_{10}S\text{-}]_2$, L^2 = 4-methylpyridine) on the surface of a gold electrode. We found that the CO ligand in the SAM is released when the triruthenium cluster center is oxidized by one electron.[13] The CO liberation process was employed to construct multilayers of the cluster on gold electrode surfaces through subsequent formation of metal–ligand coordination bonds.[14]

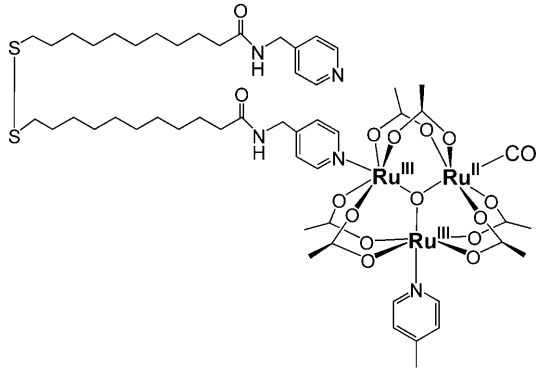

Scheme 1. Structure of the triruthenium complex. Roman numerals represent the formal Ru oxidation states.

In the present study, the oxidation states of the triruthenium cluster in the SAM (Scheme 1) are characterized by electrochemistry, in situ IR spectroscopy, and in situ sum frequency generation (SFG) vibrational spectroscopy measurements. Oxidation state-dependent reversible CO ligand exchange reactions, including CO liberation and coordination (Scheme 2), which have already been preliminarily reported by our group,[28] are realized in the SAM by tuning the electrode potential. The kinetics of both reactions has also been evaluated.

Since the synthesis of oxo-centered triruthenium complexes containing the CO ligand was established in earlier studies, CO ligand liberation upon oxidation of the triruthenium cluster center has been investigated.[19,21] It is of great interest to develop a nanostructure built from the triruthenium cluster into a novel CO sensor by combination of CO liberation and coordination processes of the cluster. In this study, following a detailed characterization of the oxidation states of the SAM during three consecutive one-electron transfers by means of electrochemistry and IR spectroscopy, a reversible exchange of the CO ligand in the SAM is realized under electrochemical control. Not only can the CO ligand be released from the CO-bound SAM (denoted as CO-SAM), to result in a CO-free SAM, but the CO ligand can also be re-coordinated to its original site in the SAM in a CO-saturated solution by electrochemically controlling the oxidation state of the triruthenium cluster center in the CO-free SAM (Scheme 2). The CO re-coordination combined with the CO liberation process establishes a reversible CO ligand-exchange cycle, which can hopefully be employed in the development of novel nanodevices capable of sensing the CO molecule in the near future.

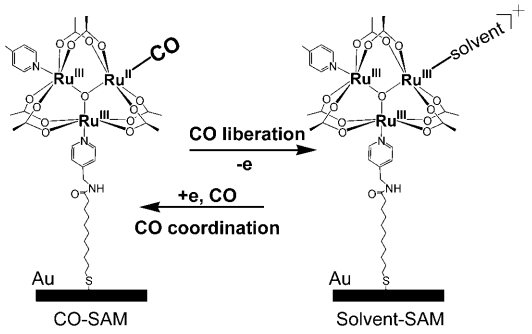

Scheme 2. Reversible CO exchange cycle in the SAM of the triruthenium cluster.

The fundamental kinetics of the CO substitution reactions, including CO coordination and the liberation of the triruthenium clusters, have rarely been reported.[13] Fixation of the triruthenium cluster onto an electrode surface provides a good opportunity to carry out a detailed kinetics study. The reaction kinetics of both processes is evaluated by in situ IR spectroscopy in the present study. Temperature and solvent effects on both CO liberation and CO re-coordination processes are also examined. Reactions rates of both processes are affected by the solvent employed and are also significantly affected by the solution temperature, which constitutes another important factor in CO exchange control.

Results and Discussion

It is well known that the triruthenium cluster $[Ru_3(\mu_3\text{-}O)(\mu\text{-}CH_3COO)_6L_3]^n$ usually shows strong electronic delocalization within the cluster.[26] Although the formal oxidation states of the triruthenium cluster center are usually expressed in different Roman numerals, such as $[Ru_3^{II,III,III}]$ or $[Ru_3^{IV,III,III}]$, in most cases, the actual oxidation states of each Ru ion in the cluster cannot be clearly distinguished owing to electronic delocalization in the system.[26] However, when the CO ligand is coordinated to the cluster, the electronic delocalization in the triruthenium cluster is significantly dis-

turbed.[21] It is known that the CO ligand, as a strong π-acid ligand, can form a strong electron donation and back-donation bond with Ru ions. As a result, only [(Ru^{II}–CO)Ru^{III}-Ru^{III}], in which the formal electron density of the Ru ion bound by the CO ligand is higher than those of the other two Ru ions, can be isolated as a stable species from a synthesis process.[29] However, the information about the oxidation state in other oxidation states of the Ru–CO cluster is still not available because these species are not stable enough to be isolated. In the present study, in situ IR measurement is employed to study the oxidation states of the Ru–CO cluster in the SAM during the multielectron transfer process. It is found that the spectroscopic and electrochemical features of the SAM and the stability of the CO ligand are closely related to the electronic localization within the cluster.

IR spectra of the complex and the SAM

Basic peak assignment: The transmission IR spectrum of the complex dispersed in a KBr disk and the IR reflection absorption spectrum of the SAM in air are shown in Figure 1a and b, respectively. In both cases, the triruthenium cluster centers are in the identical oxidation state of [(Ru^{II}–CO)-Ru^{III}Ru^{III}]^0.[13,26] In the spectrum of the complex in the KBr matrix, the stretching mode ν(CO) of the CO ligand is observed at 1942 cm^{-1}. The asymmetric stretching mode ν_{as}-(OCO) of the acetate bridges shows two absorption peaks at 1609 cm^{-1} and 1571 cm^{-1}, and the symmetric stretching mode ν_s(OCO) gives one broad peak at 1420 cm^{-1},[13,21] which shows a wider peak width than those of the ν_{as}(OCO) modes (Figure 1a and Table 1). The C=O stretching mode of the amide group gives an absorption band at 1651 cm^{-1}. In the spectrum of the SAM on the gold surface in air (Figure 1b), two new features are observed in comparison with those in the KBr matrix: 1) the absorption peak for the C=O stretching mode of the amide group is absent in the case of the SAM. According to the surface selection rule of the IR reflection absorption spectroscopy,[30] the absence of this peak indicates that the direction of the C=O stretching of the amide group must be parallel to the surface of the gold electrode, that is, the long alkyl chain in the SAM is perpendicular to the surface of the gold electrode. 2) The peak positions of the CO ligand and the acetate bridges of the SAM in air shift slightly to a higher wavenumber compared to those in the bulk crystal (Table 1). The peak shift is ascribed to the fact that the molecules exist in two different environments, that is, in the KBr matrix and in the monolayer on the surface of the gold electrode.

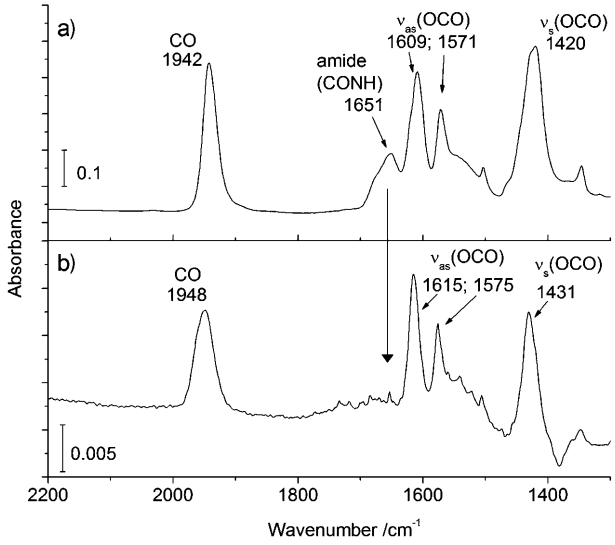

Figure 1. a) IR transmission spectrum of the triruthenium complex in a KBr matrix. b) IR reflection absorption spectrum of the monolayer self-assembled from the triruthenium complex on an evaporated gold substrate in air. Both are obtained by integrating 300 interferograms, which requires 60 s.

Table 1. IR peaks of the CO ligand and the acetate bridging ligands in the cluster with the formal oxidation state [(Ru^{II}–CO)Ru^{III}Ru^{III}]^0 in different environments.

Samples			IR absorption (Δ_{fwhm}[a]) [cm^{-1}]			
			ν(CO)	ν_{as}(OCO)	ν_s(OCO)	$\nu(CO)_{amide}$
crystalline complex in KBr matrix			1942	1609 (21), 1571 (16)	1420 (34)	1651
SAM	in air		1948	1615 (20), 1575 (15)	1431 (32)	[b]
SAM	in solution	$HClO_4/H_2O$ (0.1 M)	1960	1600, 1570	1432	[b]
SAM	in solution	$TBAPF_6$/CH_3CN (0.1 M)	1940	1610, 1576	1430	[b]
SAM	in solution	$TBAPF_6$/1,2-dichloroethane (0.1 M)	1939	1610, 1575	1430	[b]

[a] fwhm: Full width at half maximum [b] Peak of $\nu(CO)_{amide}$ in the SAM is absent.

ν_{as}(OCO) and ν_s(OCO) absorptions: It is interesting to note that IR spectra of both the complex crystal and the SAM give two peaks for ν_{as}(OCO) but only one peak for ν_s(OCO) (Figure 1). Similar phenomena have also been reported for an analogous triruthenium complex.[21,31,32] It has been suggested that the appearance of the two IR peaks of ν_{as}(OCO) is due to a lowering of the molecular symmetry of the cluster center.[21,32] However, it is still puzzling why only one peak is observed for the ν_s(OCO) mode of the acetate ligand. This phenomenon can be understood on the basis of the electron distribution in the cluster, which determines its molecular symmetry. The dipoles of the ν_{as}(OCO) and ν_s-(OCO) modes are affected by the electronic localization states in the triruthenium cluster, especially in the carbonyl triruthenium complex, which has a clear electronic localization state as [(Ru^{II}–CO)Ru^{III}Ru^{III}]^0. The stretching vibration modes of the acetate ligands coordinated to Ru^{II} and Ru^{III}

ions should show a different IR absorptions from those of the acetate ligands coordinated to two Ru^{III} ions. In the cluster, two of the six acetate bridges coordinate to two Ru^{III} ions, while four of them coordinate to Ru^{II} and Ru^{III} ions (Scheme 1). Hence two IR peaks are expected for either ν_{as}-(OCO) or ν_s(OCO) modes. It appears that the coupling interaction between the Ru^{III}–Ru^{II} intramolecular electric field and the dipole of the ν_{as}(OCO) mode seems to be stronger than that with the dipole of the ν_s(OCO) mode on account of the symmetry of the triruthenium cluster under the electron localization state of $[(Ru^{II}–CO)Ru^{III}Ru^{III}]^0$. As a result, the peak separation between two ν_{as}(OCO) modes is larger than that of the ν_s(OCO) mode. In a fully electronically delocalized state, it is anticipated that only one absorption peak should be observed for both ν_s(OCO) and ν_{as}-(OCO) since the electronic environment for all acetate bridges is the same. This observation will be discussed below for the generation of an electronic localization state in the cluster under electrochemical control.

Electrochemical behavior of the SAM: Although the multistep electron-transfer behavior of the triruthenium complex in solution has been widely studied,[13,19–21,33–35] this electron-transfer behavior of the cluster assembled as a monolayer on an electrode surface has not yet been investigated. The one-electron oxidation in the SAM has been previously investigated in aqueous solutions by our group.[13,28] In this report, the multistep electron-transfer behavior of the SAM is investigated in nonaqueous solutions in which a wider potential window is available.

The cyclic voltammogram (CV) of the SAM in acetonitrile is shown as a solid line in Figure 2. Two oxidation reactions with nearly identical charges are observed at $E_a = +0.63$ V and $+1.26$ V, which are more positive than its rest potential (ca. $+0.3$ V). Each of the two reactions has its corresponding reverse reaction and the peak separation of each redox peak is about 20 mV, indicating good reversibility. With reference to the redox peaks on the CV of the complex

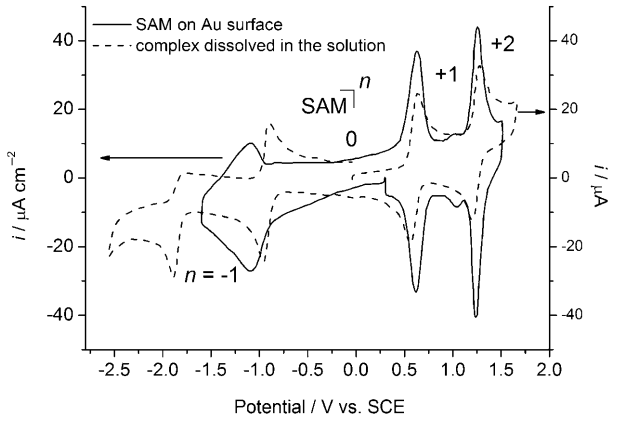

Figure 2. Cyclovoltammograms of the SAM (——, 500 mV s^{-1}) and the complex (-----, 200 mV s^{-1}) in an acetonitrile solution of $TBAPF_6$ (0.1 M) at room temperature. A glassy carbon working electrode was used for the CV measurement of the complex (1 mM).

(1 mM) dissolved in acetonitrile (dashed trace in Figure 2), the peaks at $+0.63$ V and $+1.26$ V from the SAM are in similar positions with respect to the two oxidation peaks of the complex in solution, which are assigned to the first one-electron oxidation $[(Ru^{II}–CO)Ru^{III}Ru^{III}]^0/[Ru_3^{III,III,III}–CO]^+$, and the second one-electron oxidation $[Ru_3^{III,III,III}–CO]^+/[Ru_3^{III,III,IV}–CO]^{2+}$, respectively.[13,35] The peak currents of the SAM increase linearly with increasing scan rate, indicating that the current observed in the CV is caused by the reaction of the redox center fixed on the electrode surface.

Baumann et al. pointed out that the presence of the CO ligand has a significant effect on the electrochemical oxidation potential of the triruthenium cluster in the bulk phase.[21] The potential for the one-electron oxidation of a CO-bound cluster is $+0.67$ V, which is more positive than that of a tris(pyridine) Ru cluster in solution. The effect is attributed to electron localization caused by the CO ligand: backdonation from the Ru ion to the CO ligand withdraws electron density from the cluster.[21] An almost identical electron localization effect is also observed in the SAM (Figure 2), which indicates similar oxidation behavior of the cluster in the bulk phase.

The charge of the one-electron oxidation peak ($+0.63$ V) was integrated to estimate the surface coverage of the SAM with Ru moiety on the surface of the gold electrode. This yields a value of about $1.1(\pm0.1)\times10^{-10}$ mol cm^{-2}, which is similar to our previous reports.[13] Considering that the disulfide ligand $[(NC_5H_4)CH_2NHC(O)(CH_2)_{10}S-]_2$ adsorbs on the gold surface through a Au–S bond while one of them is electrochemically inactive (Scheme 1), the total coverage of the surface species should be about 2.2×10^{-10} mol cm^{-2}. This coverage is much lower than that of the SAM of decanethiol, $CH_3(CH_2)_9SH$, on the surface of a gold electrode (ca. 8×10^{-10} mol cm^{-2}),[5] and this should be related to the large size (ca. 10 Å diameter) of the terminal Ru cluster in the present SAM.

The SAM also gives a broad redox peak at about -1.10 V (Figure 2, solid line), which is about 0.15 V more negative compared to that of the one-electron reduction $[Ru_3^{II,II,III}–CO]^-/[(Ru^{II}–CO)Ru^{III}Ru^{III}]^0$ of the complex in solution at $E_c = -0.96$ V (dashed line, Figure 2). In situ IR spectra of this process provide further evidence for a reduction process of the triruthenium cluster center. On the other hand, the coverage of the SAM estimated from the CV peaks largely decreases when the negative limit of the potential sweep becomes more negative than -1.1 V. Previous studies indicated that *n*-alkanethiol monolayers on gold can be desorbed in both aqueous and nonaqueous solutions under electrochemical reduction in the negative potential region.[36,37] An electrochemical quartz crystal microbalance (EQCM) study showed that the SAM of decanethiol, which has a similar length to the triruthenium cluster monolayer here, desorbed from the electrode surface at a potential more negative than -1.3 V in an acetonitrile solution.[37] If one considers the relatively low coverage of the Ru SAM in the present study, it is reasonable that the Ru SAM here could start to desorb from the surface of the gold electrode at more positive po-

tentials, for example, −1.1 V, in the region where the one-electron reduction of the Ru cluster also takes place.

The irreversible second one-electron reduction $[Ru_3^{II,II,II}–CO]^{2-}/[Ru_3^{II,II,III}–CO]^{-}$ of the complex in solution, which occurs at $E_c = -1.90$ V (dashed line, Figure 2), is not observed in the SAM because the SAM is already desorbed when the potential is swept in such a negative potential region.

Detailed electrochemical results of the SAM as well as the complex are summarized in Table 2. The electron-transfer behavior of the triruthenium cluster monolayer is a good example of reversible multistep electron transfer in monolayers on surfaces, which is still rarely reported in the literature.[38–40]

Table 2. CV data of the SAM and the complex (1 mM) in $TBAPF_6$/CH_3CN (0.1 M). Scan rates were 500 mV s^{-1} and 200 mV s^{-1} for the SAM and the complex, respectively.

Redox processes		+2/+1	+1/0	0/−1	−1/−2
$[SAM]^n$	E_a[a] [V] vs. SCE	+1.26	+0.63	−1.08	
	E_c[b]	+1.24	+0.61	−1.10	
	$E_{1/2}$[c]	+1.25	+0.62	−1.09	[f]
	ΔE_p[d] [mV]	20	20	20	
	ΔE_{fwhm}[e] [mV]	120	150	260	
Complex (1 mM)	$E_{1/2}$	+1.24	+0.60	−0.93	−1.90
	ΔE_p [mV]	80	80	60[g]	

[a] Anodic peak potential versus SCE. [b] Cathodic peak potential. [c] Calculated from the averages of anodic and cathodic peak potentials. [d] Peak-to-peak separation. [e] Full width at half maximum obtained from anodic peaks. [f] The second electron reduction can not be observed in the SAM. [g] Irreversible process, a reduction wave only.

In situ IR characterization of the oxidation states of the SAM: The triruthenium complex containing the CO ligand can only be isolated in the formal oxidation state of $[(Ru^{II}–CO)Ru^{III}Ru^{III}]^0$ owing to its high stability induced by the strong backdonating nature of the Ru into the π^*-antibonding orbital of CO ligand.[21,26,41] The Ru–CO complex in other oxidation states is not stable enough to be evaluated by means of conventional ex situ techniques. To investigate the structural changes and oxidation states of the SAM during successive redox cycles, we employed in situ IR measurements, which have a high time resolution and are sensitive enough to monitor the reactions of monolayers.[42–45] The use of in situ IR spectroscopy provides rich structural information on the SAM in different oxidation states, which is impossible to obtain by conventional electrochemical measurements.

In situ IR spectra were obtained by subtraction, that is, a background measured at a reference potential was subtracted from a sample spectrum at a target potential. In absorbance units, IR absorptions in sampling states produce upward peaks, while IR absorptions in background states produce downward peaks. IR spectra for sampling states of $n = +1$, $+2$, and -1 referenced to a background spectrum in the original state ($n = 0$) of the SAM in an acetonitrile solution at +0.3 V are shown in Figure 3a, b, and c, respectively. Downward peaks at $\tilde{\nu} = 1940$, 1610, 1576, and 1430 cm^{-1} are observed in all three spectra, corresponding to the IR absorptions of the original $[(Ru^{II}–CO)Ru^{III}Ru^{III}]^0$ in the SAM. Based on the peak assignments of the complex and the SAM in the same oxidation state, the three peaks are assigned to ν(CO), ν_{as}(OCO) (doublet), and ν_s(OCO), respectively. The positions of these peaks are influenced by the solvent used (Table 1). CV measurement in 1,2-dichloroethane gives almost identical peak positions as those observed in acetonitrile. As shown in Table 1, ν(CO) shifts to a higher wavenumber, while ν_{as}(OCO) shifts to a lower wavenumber, and ν_s(OCO) remains in nearly the same position in an aqueous solution with respect to those obtained in a nonaqueous solution. The effect of the solvent on the IR absorption frequencies of solutes is complicated, and its mechanism is still not well understood. Previous studies show that

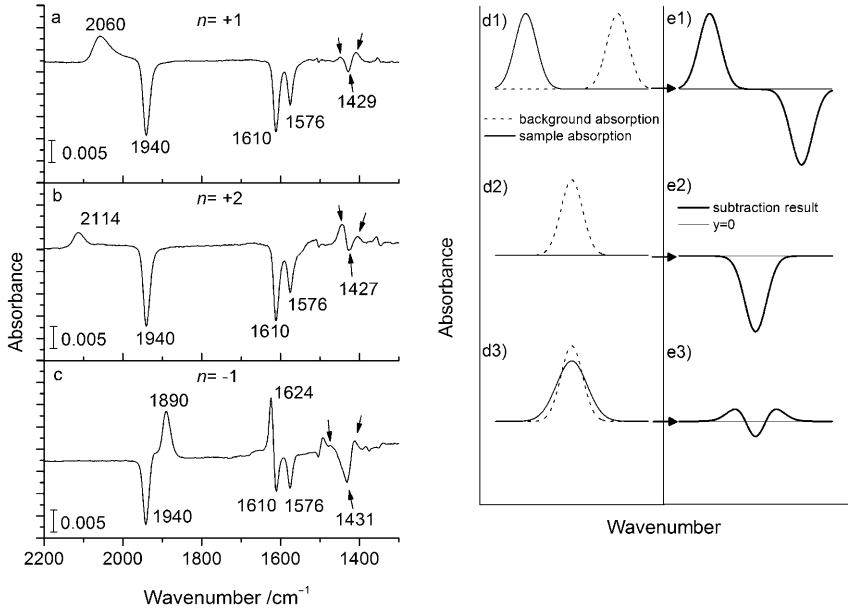

Figure 3. IR spectra of the SAM in different oxidation states in an acetonitrile solution of $TBAPF_6$ (0.1 M). Spectra a, b, and c were recorded at +0.8 V, +1.55 V, and −1.6 V, respectively. The background spectrum was recorded at +0.3 V. Upward and downward peaks represent the species in sample and in the background state respectively. All the spectra are integrated from 15 interferograms over 3 s. Simulated spectra for the peak shift: only downward peaks and triplet features are given in d1/e1, d2/e2, and d3/e3, respectively. Spectra d are generated from the function $y = A\exp\left[-\frac{(x-x_c)^2}{2w^2}\right]$ (A amplitude, x_c center, $2w = w_1/\sqrt{\ln 4}$, w_1 full width at half maximum). The spectra in e1–e3 were generated by subtracting the background from the sample in d1–d3, respectively.

electrostatic interaction between the solvent and the solute affects the IR frequency of the solute, which indicates that the dielectric constant of the solvent is an important factor.[46–48] Here, the interaction between the solvent and the SAM is considered to be the main reason for the difference in the positions of the IR peaks. IR peak shifts caused by solvent or environment effects are totally different from those caused by redox processes in the triruthenium cluster center, as observed in the in situ IR spectra.

ν(CO) peak in each oxidation state: Different upward IR peaks were recorded in three different oxidation states. The ν(CO) peak, which is located at 1940 cm^{-1} in $n = 0$, shifts to 2060 cm^{-1}, 2114 cm^{-1}, and 1890 cm^{-1} in $n = +1$, $+2$ and -1, respectively (Figure 3a, b and c). The blue-shift of the CO peak position means the strengthening of the ν(CO) vibration, which can be attributed to the weakening of the dπ(Ru)–π*(CO) electron backdonation owing to electron redistribution during the oxidation of the triruthenium cluster center.[35] The one-electron reduction, which increases the electron density in the triruthenium cluster center and therefore, increases the electron backdonation from the Ru ions to the CO ligand, leads to the shift of the peak to a lower wavenumber.

A detailed comparison of the IR peaks of the CO ligand in different oxidation states (Table 3) shows two important features: 1) among the three one-electron transfer processes, the CO peak shift of the one-electron oxidation $[(Ru^{II}–CO)Ru^{III}Ru^{III}]^0/[Ru_3{}^{III,III,III}–CO]^+$ is nearly 120 cm^{-1} and is much larger than the other two which are about 50 cm^{-1}. This feature indicates that the one-electron oxidation takes place at the Ru^{II} site directly bound by the CO ligand. Because the other two redox process ($+2/+1$, $0/-1$) can only induce a shift of the CO peak by about 50 cm^{-1}, it is suggested that the Ru-CO cluster in the SAM changes its electronic localization state $[(Ru^{II}–CO)Ru^{III}Ru^{III}]^0$ to the delocalization states in $[Ru_3{}^{II,II,III}\text{-}CO]^-$, $[Ru_3{}^{III,III,III}–CO]^+$, and $[Ru_3{}^{IV,III,III}–CO]^{2+}$ after the redox process of the Ru central ions in the cluster. 2) The peak width of the CO ligand at $[Ru_3{}^{III,III,III}–CO]^+$ is about 40 cm^{-1}, which is nearly twice that of the other three states (ca. 20–25 cm^{-1}). The broader CO peak at the one-electron oxidation state indicates a wider state distribution of the CO ligand than the other three states. It is possible that there is a partial electronic localization state, such as $[(Ru^{II}–CO)Ru^{III.5}Ru^{III.5}]^+$, even in the $[Ru_3{}^{III,III,III}–CO]^+$ state owing to the strong coordination ability of the CO ligand with the Ru ion. As discussed below, the electronic localization/delocalization state in the Ru–CO cluster greatly affects the binding state of Ru–CO and the stability of the CO ligand, resulting in the liberation of the CO ligand.

Table 3. IR data of the SAM in $TBAPF_6/CH_3CN$ (0.1 M) and $HClO_4/H_2O$ (0.1 M).

Redox of the $[SAM]^n$: $n/(n-1)$	$+2/+1$		$+1/0$	$0/-1$
solvent	CH_3CN	CH_3CN	aqueous solution	CH_3CN
CO peak in $n/(n-1)$ [cm^{-1}]	2112/2058	2058/1940	2070/1960	1940/1890
peak shift of redox [cm^{-1}]	54	118	110	50
Δ_{fwhm}[a] in $n/(n-1)$ [cm^{-1}]	25/40	40/20	55/25	20/20

[a] fwhm: Full width at half maximum.

$\nu_{as}(OCO)$ and $\nu_s(OCO)$ peaks in each oxidation state: The changes of the acetate bridge peaks are quite different and more complicated than the changes of the CO ligand peak induced by the three redox processes. As described above, IR measurements can only probe the relative structural change to the background state since subtraction of the background is always necessary. In order to understand the complicated spectral features of the acetate bridges as well as those of the CO ligand observed in the different oxidation states, spectral subtractions simulations were carried out (d and e in Figure 3). Assuming that all IR absorptions follow Gaussian functions (see the legend to Figure 3), IR subtractive spectra e1–e3 were reproduced by subtracting the background absorption from the sample absorption in spectra d1–d3, respectively. Spectrum e1 exhibits a peak shift similar to those of CO observed in spectra a–c is well reproduced.

The simulation for the acetate bridge (e2 and e3 in Figure 3) is slightly complicated. As shown in a and b of Figure 3, ν_{as}(OCO) of the acetate bridges shows no upward peaks in the two oxidized states $[Ru_3{}^{III,III,III}–CO]^+$ and $[Ru_3{}^{IV,III,III}–CO]^{2+}$, indicating that the IR absorption at 1610 cm^{-1} and 1576 cm^{-1} becomes weak or even disappears after one-electron oxidation or two-electron oxidation. This situation is simulated in Figure 3, d2 and e2. To confirm the assumption made in the simulation, in situ SFG measurements were carried out in the states

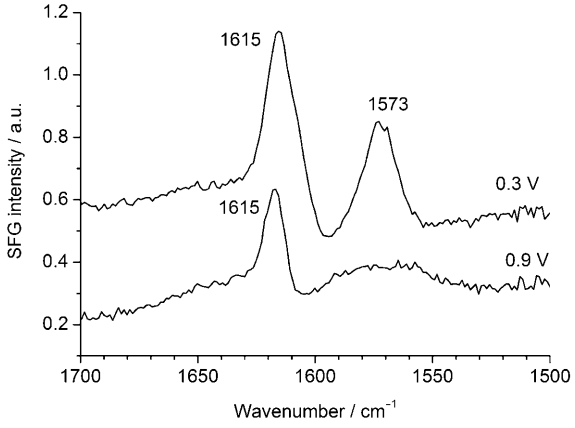

Figure 4. In situ sum-frequency generation (SFG) spectra of the SAM in the frequency region of the ν_{as}(OCO) vibration at $+0.3$ V and $+0.9$ V, respectively. Each spectrum is co-added over 100 s.

$[(Ru^{II}–CO)Ru^{III}Ru^{III}]^0$ and $[Ru_3^{III,III,III}–CO]^+$, as shown in Figure 4. As a second-order nonlinear vibrational technique, SFG measurement demonstrates high surface selectivity and sensitivity, and can directly give an absolute vibrational spectrum thus avoiding any confusion arising from subtraction of the background.[49–51] The SFG spectrum of the ν_{as}-(OCO) at +0.3 V shows two peaks at 1615 cm^{-1} and 1573 cm^{-1}, which agree well with both the ex situ and in situ IR results. When the Ru cluster center is one-electron oxidized to $[Ru_3^{III,III,III}–CO]^+$ at +0.9 V, the peak at 1615 cm^{-1} decreases to nearly half intensity and the peak at 1573 cm^{-1} almost disappears. This result proves that the simulation made above is reasonable, namely one of the IR absorptions of ν_{as}(OCO) becomes weaker and another one disappears after one-electron oxidation at +0.9 V. On the other hand, an ex situ IR measurement also demonstrated that the ν_{as}-(OCO) absorption of the triruthenium complex $[Ru^{III}{}_3(\mu_3\text{-}O)(\mu\text{-}CH_3COO)_6(L)_3]^+$ (L: H_2O or pyridine), which has an identical oxidation state to $[Ru_3^{III,III,III}–CO]^+$, was significantly weakened, although the CO ligand is absent in this case.[32] Based on the discussion above, when the electron density in the Ru cluster is fully delocalized among the three metal centers, all six acetate ligands are in an identical electronic environment and there is only one absorption peak for the ν_{as}(OCO) mode, as in Figure 4.

In the case of the reduced state $[Ru_3^{II,II,III}–CO]^-$, an upward peak is observed at 1624 cm^{-1} in addition to two downward peaks at 1610 cm^{-1} and 1576 cm^{-1} for ν_{as}(OCO) absorption (Figure 3c). This indicates two issues: 1) ν_{as}-(OCO) still has a comparable IR absorption intensity after the reduction process, although the peak position is shifted. 2) Only one upward peak suggests that all the acetate ligands are in a similar electronic environment, that is, the electron density is delocalized in the cluster in the state of $[Ru_3^{II,II,III}–CO]^-$. This conclusion also agrees with the above discussions for the CO ligand.

On the other hand, ν_s(OCO) shows more complicated features compared to those observed for ν_{as}(OCO). A triplet, which occurs as a downward peak in the center of two peaks, is observed near the ν_s(OCO) position at 1430 cm^{-1} in each charged state (Figure 3c). As shown in Figure 3 (e3), this triplet shape may result from the subtraction of a slightly decreased and broadened absorption peak from the original one. The absorption of ν_s(OCO) is not affected as significantly by redox processes of the triruthenium cluster center compared to that of ν_{as}(OCO). Detailed reasoning for this is still under investigation.

Dynamic observation of the first one-electron oxidation process: A series of IR spectra were recorded concurrently with the potential sweeping from +0.1 V to +0.9 V and then back to +0.1 V at a scan rate of 20 mV s^{-1} (Figure 5a). The background spectrum was recorded at +0.1 V and the sampling was started at +0.1 V with an interval of 60 mV. Flat IR spectra were observed until +0.46 V, indicating that no structural change takes place in the SAM. After +0.46 V, a downward peak at 1940 cm^{-1} of CO in the original state and

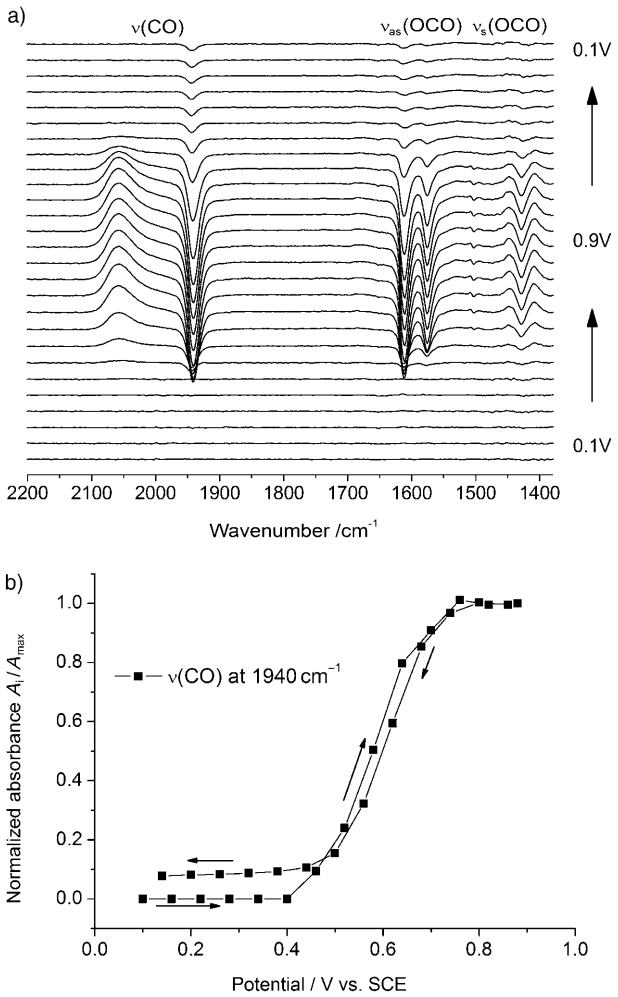

Figure 5. a) Series of time-resolved IR spectra of the SAM on an Au electrode surface collected sequentially during a potential sweep from +0.1 V to +0.9 V and back to +0.1 V at a scan rate of 20 mV s^{-1} in acetonitrile with $TBAPF_6$ (0.1 M). The time resolution is 3 s, that is, the sampling interval is 60 mV. Each spectrum is co-added from 15 interferograms. The background spectrum was recorded at +0.1 V. b) Variation of the normalized IR peak of CO (1940 cm^{-1}) intensity (A_i/A_{max}) with potential sweeping as in part a. A_i represents the IR peak intensity of CO in each spectrum in part a, and A_{max} is the maximum value.

the upward peak at 2060 cm^{-1} of CO in the oxidized state appear and their intensities increase as the potential is swept positively, indicating that the oxidation of the triruthenium complex greatly affects the state of the CO ligand, as discussed above. The intensities of the downward peaks of ν_{as}(OCO) at 1610 cm^{-1} and 1576 cm^{-1} as well as the triplet feature of ν_s(OCO) around 1430 cm^{-1} also increase as the potential is swept from +0.46 V to +0.9 V. As the potential is swept back from +0.9 V to +0.1 V, all the peaks begin to decrease. The evolution of IR spectra shows good agreement with the redox process in the SAM. However, very small downward peaks can still be observed for ν(CO), ν_{as}(OCO), and ν_s(OCO) after the potential has returned to +0.1 V. The normalized IR peak intensity of the CO ligand at 1940 cm^{-1} as a function of the electrode potential is

shown in Figure 5b. When the potential returns to +0.1 V, the CO peak intensity does not return to zero, indicating that a small amount of CO ligand or Ru cluster may be lost after one CV cycle of the one-electron redox process with a scan rate of 20 mV s^{-1}. The IR spectra confirm the previous electrochemical observations that the one-electron oxidation of the triruthenium complex either in solution or assembled as a monolayer on an electrode surface triggers a CO liberation process.[13,21] This will be discussed in detail in the next section.

Reversible CO ligand exchange cycle in the SAM

CO liberation process: The liberation of CO upon one-electron oxidation of the SAM in an aqueous solution was observed previously by electrochemical characterization.[13] Here, the change in the CO ligand in the SAM in the nonaqueous solution is monitored by CV and in situ IR measurements with the potential held at +0.9 V, whereby the SAM was oxidized to $[Ru_3^{III,III,III}–CO]^+$. As shown in Figure 6a, sequential changes are observed for a series of CVs from A to K, while in situ IR spectra are sampled concurrently with electrolysis with an interval of 2 min. The two redox peaks of the SAM at +0.62 V and +1.25 V in cyclic voltammogram A decrease as the electrolysis time increases, while two new redox peaks at +0.01 V and +1.05 V increase. The arrows in the figure represent the direction of change. After the potential was kept at +0.9 V for one hour, cyclic voltammogram A changed to cyclic voltammogram K. The charges of the new redox peaks at +0.01 V and +1.05 V are almost identical to those of the two redox peaks at +0.62 V and +1.25 V, which disappear after electrolysis.

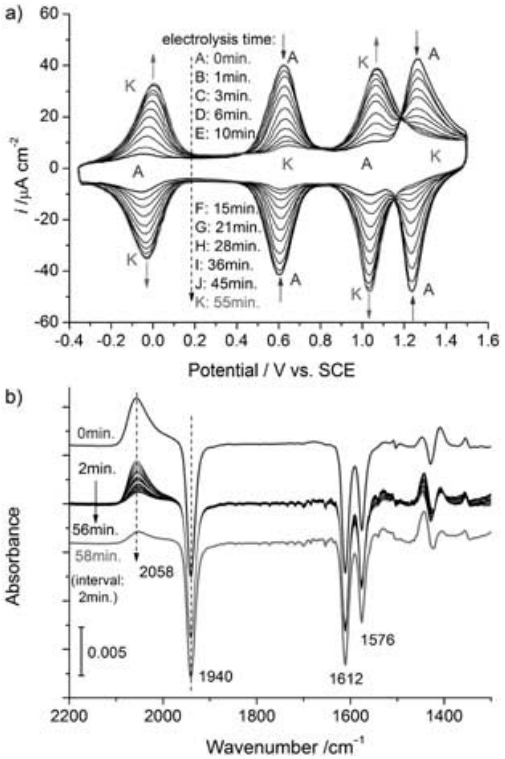

Figure 6. a) Various CVs of the SAM on a gold surface recorded in $TBAPF_6/CH_3CN$ (0.1 M) at a scan rate of 500 mV s^{-1} with the electrolysis times increasing in the sequence shown. Lines A and K represent the CV of the original CO-SAM and the CV of the CO-free SAM, that is, solvent-SAM, respectively. The electrode potential was held at +0.9 V in which the triruthenium cluster center is in the $[Ru_3^{III,III,III}–CO]^+$ state. b) In situ IR spectra of the SAM measured during the electrolysis process with the potential kept at +0.9 V. The background was recorded at +0.3 V. Each spectrum was integrated from 300 interferograms over 60 s.

The IR spectrum of the SAM prior to the electrolysis process (0 min) is identical to that shown in Figure 3a, indicating one-electron oxidization of the SAM to the $[Ru_3^{III,III,III}–CO]^+$ state. As the electrolysis time increases, the IR peak at 2060 cm^{-1}, assigned to the ν(CO) absorption in $[Ru_3^{III,III,III}–CO]^+$, decreases sequentially. The doublet peaks of the ν_{as}(OCO) at 1612 cm^{-1} and 1576 cm^{-1} do not change in shape or in intensity, and the peak of ν_s(OCO) still presents itself as a triplet shape and does not change much in intensity. However, a small upward peak at 1448 cm^{-1} increases with electrolysis time in comparison with other two peaks, indicating that the position of ν_s(OCO) in the oxidation state shifts slightly to a higher wavenumber. The in situ IR spectra of the acetate ligand indicate that the main structure of the triruthenium cluster center is maintained, but the CO ligand is released from the monolayer when the surface immobilized cluster is electrochemically controlled as $[Ru_3^{III,III,III}–CO]^+$. The weakening of the dπ–π* backdonation caused by the oxidation process is expected to contribute to this CO liberation process.[13,21] After the CO liberation process, the CO-SAM is changed to a CO-free SAM.

An interesting issue is what has happened on the Ru site originally bound by CO after electrolysis. A conventional explanation is that solvent molecules take the place of CO and bind to the Ru center. Baumann et al. proposed that solvent molecules, such as acetonitrile or dichloromethane, could occupy the vacant coordination site following oxidation of $[Ru_3(\mu\text{-}O)(CH_3COO)_6(CO)(py)_2]^+$ in acetonitrile or dichloromethane solution because they could isolate an acetonitrile complex $[Ru_3(\mu\text{-}O)(CH_3COO)_6(CH_3CN)(py)_2]^+$.[21] In the case of the SAM here, it would be expected that the IR absorption of the C–N stretching, ν(CN), would appear if acetonitrile replaced CO and bound to the Ru center. However, ν(CN) was not observed by the present in situ IR experiment. Two possible reasons are considered at this stage.

The first possibility is that ν(CN) may become very weak, even though CH_3CN is coordinated to the Ru center. It has been reported that the IR absorption intensity of the nitrile stretching vibration is strongly affected by the coordinated group.[52,53] When electronegative groups are coordinated to the *C* terminus of the nitrile group, the nitrile absorption becomes very weak or absent.[52] As an example, the Supporting Information contains an IR spectrum of the complex $[Ru_2(\mu\text{-}O)(\mu\text{-}CH_3COO)_2(bpy)_2(CH_3CN)](PF_6)_2$, in which acetonitrile is known to coordinate to the Ru center by the N terminus, as confirmed by XRD and NMR measurements.

However, it is hard to see the ν(CN) band from acetonitrile and only strong absorptions from acetate bridges are observed. A contrary case was observed by Zavarine et al. for the triruthenium cluster bound to the *C* terminus of isocyanide ligands as $[Ru_3(\mu\text{-}O)(\mu\text{-}CH_3COO)_6(L)_3]$ (L = xylyl isocyanide or *tert*-butyl isocyanide).[54] The IR peak of the isocyanide group exhibits strong oxidation state dependence, which is similar to the present case of the CO ligand in the SAM here. Therefore, it is possible that the absorption of the nitrile group in the SAM here can be weakened as the electropositive group of the Ru^{III} center is coordinated to the *N* terminus of the nitrile group.

The second possibility is that the interaction between the acetonitrile and the Ru center may be very weak. Baumann et al. noted that the solvent molecules are weakly bound in the solvent complex $[Ru_3(O)(CH_3COO)_6(solvent)_3]^+$, and they are easily replaced by a variety of ligands.[21] Because the interaction between the acetonitrile and Ru center is very weak, ν(CN) may be not significantly affected by the change in the oxidation state of the Ru centers. Therefore, it may be reasonable that no peak for ν(CN) is observed in the subtractive in situ IR spectra. The interaction between the acetonitrile and Ru center may not be a real chemical bond as is the case for the CO ligand. Although an acetonitrile complex $[Ru_3(\mu\text{-}CH_3COO)_6(CH_3CN)(py)_2]^+$ was isolated by Baumann et al., the possibility of a crystallized solvent molecule in the complex can not be ruled out. The interaction between the solvent molecule and the Ru center is a fundamental and interesting subject in inorganic chemistry, and further study is still being carried out in our laboratory.

Herein, the CO-free SAM is annotated as solvent-SAM for brevity. As shown by its CV (line K, Figure 6a) in a nonaqueous solution, the solvent-SAM also exhibits multistep electron-transfer behavior. By comparison with the redox peaks of a similar complex $[Ru_3(\mu_3\text{-}O)(CH_3COO)_6(mpy)_2(solvent)]ClO_4$ (mpy = 4-methylpyridine) in acetonitrile solution, the new redox peaks at +0.01 V and +1.05 V are assigned to redox couples of $[Ru_3^{II,III,III}\text{–solvent}]^0/[Ru_3^{III,III,III}\text{-solvent}]^+$ and $[Ru_3^{III,III,III}\text{–solvent}]^+/[Ru_3^{IV,III,III}\text{–solvent}]^{2+}$ in the SAM, respectively.[34] The charges of the two redox processes are identical. The conversion ratio from solvent-SAM to CO-SAM can be estimated by comparing the surface charge of solvent-SAM to that of CO-SAM. After electrolysis for 1 h, about 90% of the initial carbonyl complex assembled on the gold surface was converted to a CO-free one, which means that the surface coverage of solvent-SAM is about 0.9×10^{-10} mol cm^{-2}, while 5% remains as the CO-SAM, and the other 5% remaining may be desorbed from the gold surface.

CO re-coordination: Reintroduction of CO into the SAM is of great interest because it can be combined with the CO liberation process to form a novel CO exchange cycle in the monolayer. Although the synthesis of a triruthenium complex containing a CO ligand has been achieved,[19,21] introducing a CO ligand into the monolayer of the triruthenium complex has not yet been realized.

The first attempt was carried out by introducing CO gas into the aqueous or nonaqueous solution under open circuit conditions with a rest potential of about +0.3 V, whereby the solvent-SAM is in the $[Ru_3^{III,III,III}\text{–solvent}]^+$ state. The experimental results in an aqueous solution are shown in Figure 7. CV and in situ IR spectra of the original CO-containing SAM and the CO-free SAM are shown as Figure 7a1 and b1, and Figure 7a2 and b2, respectively. After maintaining CO saturation of the solution for 1 h, no change was observed in either the CV or the IR spectra (Figure 7a3 and b3), indicating that it is difficult for CO to react with the triruthenium cluster monolayer in the state $[Ru_3^{III,III,III}\text{–solvent}]^+$. Similar results were also observed in acetonitrile and 1,2-dichloroethane solutions.

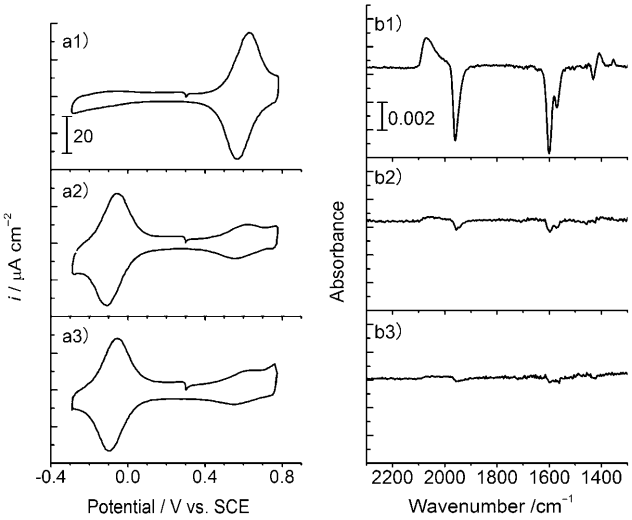

Figure 7. CV and IR spectra of the SAM of the triruthenium cluster in the aqueous solution of $HClO_4$ (0.1 M). a1 and b1: original SAM containing CO; a2 and b2: after electrolysis at 0.8 V for 20 min; a3 and b3: after introduction of CO gas at the rest potential (+0.3 V) for 1 h. Scan rate of CV is 500 mV s^{-1}. Potentials of IR sample and background spectra are +0.8 V and +0.3 V, respectively. Each spectrum was obtained by co-adding 15 interferograms over 3 s.

Considering that the CO-bound Ru ion site in the CO-SAM is only stable in the Ru^{II}–CO state, the solvent-SAM is subjected to a one-electron electrochemical reduction by controlling the electrode potential at −0.3 V to trap CO on the Ru^{III}-solvent site. Surprisingly, this electrochemical control leads to re-coordination of the CO ligand, as confirmed both by the CV and in situ IR spectra. A series CVs, from lines A–K in Figure 8a, were recorded sequentially in a CO-saturated acetonitrile solution while the potential was held at −0.3 V. Both redox peaks at +0.01 V and +1.05 V, which are assigned to the two consecutive one-electron transfer processes of the solvent-SAM, begin to decrease over time, while two other redox peaks significantly increase at the positions corresponding to those of the CO-SAM (+0.62 V and +1.25 V). IR spectra recorded concurrently referenced to the background taken at the same potential of −0.3 V prior to the introduction of CO gas also showed a dramatic change, as illustrated in Figure 8b. The in situ IR spectrum taken 2 min after CO gas was introduced into the solution is

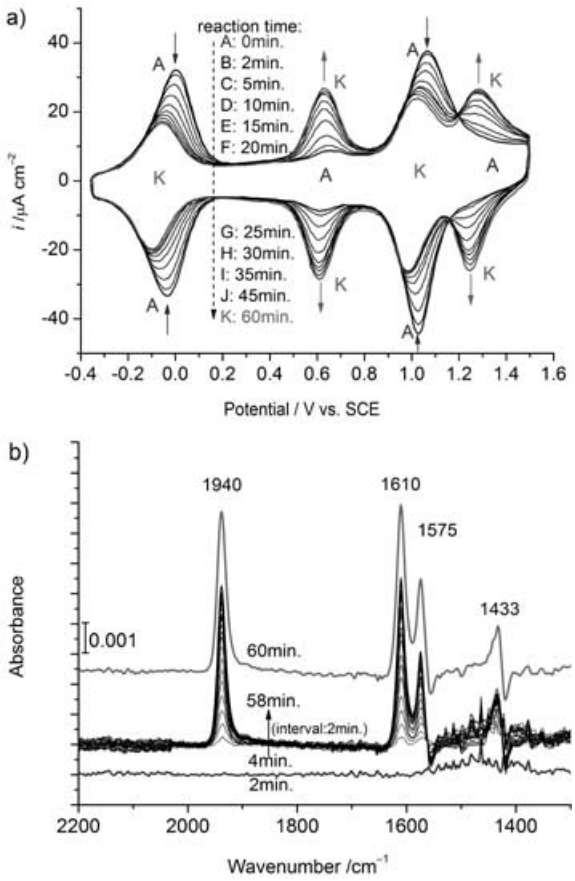

Figure 8. a) CVs recorded during the CO re-coordination process of the SAM in $TBAPF_6/CH_3CN$ (0.1 M) at a scan rate of 500 mV s^{-1}. Each line from A to K was obtained at the reaction times shown inside the figure. The electrode potential was held at −0.3 V, at which the triruthenium cluster center is in the $[Ru_3^{II,III,III}$–solvent$]^0$ state. b) In situ IR spectra of the SAM during the CO re-coordination process. The background was recorded at −0.3 V. Each spectrum is integrated from 300 interferograms over 60 s. Increases in the CO peak at 1940 cm^{-1} as well as in the peaks of the acetate bridges confirms that the solvent-SAM has converted to the CO-SAM.

still an almost flat line, that is, no change has yet taken place. However, after 4 min, four IR peaks at 1940 cm^{-1}, 1610 cm^{-1}, 1575 cm^{-1}, and 1433 cm^{-1} emerge and gradually increase. A comparison of the IR spectra of the SAM shown in Figure 1b and Figure 3a, allows the exact assignment of these peaks to ν(CO), ν_{as}(OCO), and ν_s(OCO) of the CO-SAM. Combining the results of the CV and in situ IR spectra, it is clear that the CO molecule dissolved in the solution binds to the triruthenium cluster exactly at the Ru^{II}–solvent site, which is reduced from Ru^{III}–solvent in the solvent-SAM, and the solvent-SAM has been converted to CO-SAM in the formal $[(Ru^{II}–CO)Ru^{III}Ru^{III}]^0$ state.

By comparing the charges of the redox peaks at +0.01 V of line A and +0.62 V of line K (Figure 8a), which were recorded prior to the reintroduction of CO and at 60 min after the reaction, respectively, about 56% of the solvent–SAM was recovered as CO–SAM, while 26% remained as the solvent–SAM. The remainder may be desorbed or damaged. Compared to the initial charge of the CO–SAM before the CO liberation process, about 50% of the triruthenium species were exchanged back to the CO–SAM and ≈23% are in the solvent–SAM state after this CO exchange cycle described above. This CO ligand coordination triggered by electrochemical control in the SAM is very clean, facile, and efficient in comparison with the CO ligand-coordination reaction of the triruthenium complex dissolved in the solution, which requires chemical reduction of the metal cluster by hydrazine.[21]

Reversible CO exchange in the SAM: The reversibility of the CO ligand-exchange cycle, including the liberation and recoordination steps, has been examined. The electrochemical control method described above was used to achieve up to 9 consecutive CO ligand-exchange cycles in aqueous solution (Figure 9a and b). The CO was reversibly switched on and

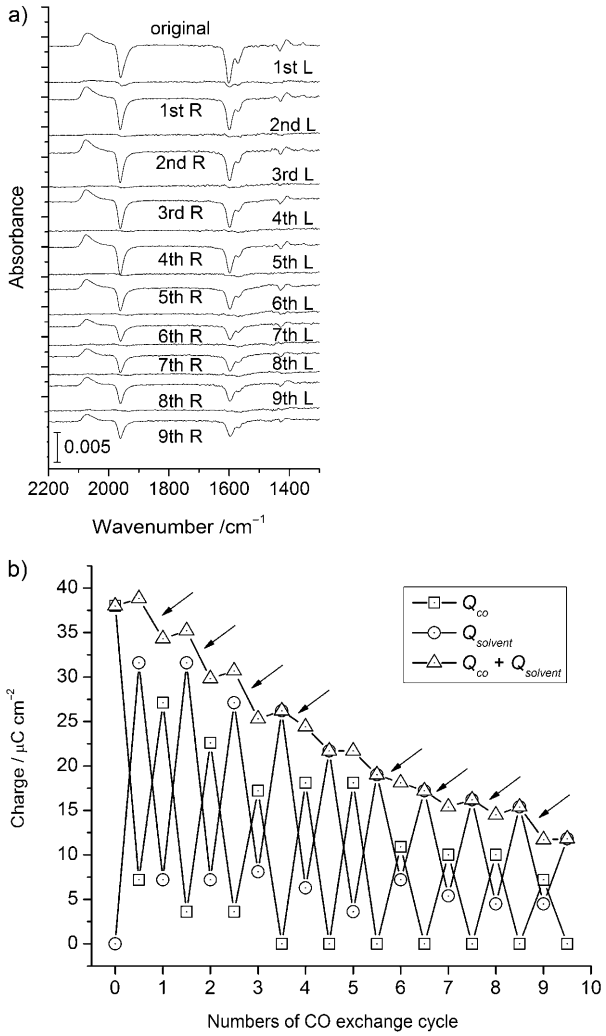

Figure 9. a) IR spectra recorded after each CO liberation and recovery step in 9 consecutive CO exchange cycles in an aqueous $HClO_4$ solution (0.1 M). The sample and background potential are +0.9 V and +0.3 V, respectively. Annotation L and R represent liberation and recovery respectively. Each spectrum is integrated from 15 interferograms over 3 s. b) Variation of the charges of the CO species (Q_{co}), solvent species ($Q_{solvent}$) and the sum (Q_{co} + $Q_{solvent}$) during the 9 CO exchange cycles. Arrows indicate the loss of the surface species.

off the triruthenium cluster monolayer. After nine CO exchange cycles, about 50% of the surface species remain active, as estimated from the CO peak intensity in the IR spectrum (Figure 9a). The charges of the CO-bound species (Q_{co}), the solvent-bound species ($Q_{solvent}$), and the sum ($Q_{co} + Q_{solvent}$) after each reaction step are summarized in Figure 9b. The gradually decreasing surface charge ($Q_{co} + Q_{solvent}$) with increasing cycle number indicates that the quantity of surface species decreases gradually in such a long-term reaction process. Two possible reasons are considered for the loss of the surface species: 1) in a previous kinetics study of the pyridine/[D_5]pyridine (C_5D_5N) ligand-exchange reaction, the rate constant of the reaction in a triruthenium cluster $[Ru_3^{II,III,III}(O)(CH_3CO_2)_6(pyridine)_3]^0$ was determined to be $2.1\times10^{-3}\ s^{-1}$ in CD_3CN and was approximately two-orders of magnitude larger than that in $[Ru_3^{III,III,III}(O)(CH_3CO_2)_6(pyridine)_3]^+$ in CD_3CN ($5.0\times10^{-5}\ s^{-1}$) under identical conditions.[41] During the process of introducing CO into the $Ru_3^{II,III,III}$ cluster, the Ru–pyridyl bond, which tethers the cluster core to the alkyl moiety, can dissociate and lead to the disconnection of the cluster from the backbone of the SAM. From the variation of ($Q_{co} + Q_{solvent}$) with cycles numbers in Figure 9b, almost all the loss occurs after the CO re-coordination step, as indicated by arrows in the figure. This supports the assumption made above. 2) It is possible that the molecule assembled on the gold substrate could be desorbed from the surface of the gold electrode during the repeated potential control processes. However, since the double layer charge of the electrode from the CV does not change much after consecutive exchange cycles, the second possibility may be less likely and the first one is more likely to dominate the loss of surface species.

Kinetics of CO liberation and coordination: There are a few kinetic studies of ligand coordination reactions in triruthenium complexes in solution.[41,55–57] The reaction rate constant of CO liberation in the triruthenium cluster monolayer was previously carried out by evaluating the change of the peak charge in the CV with respect to the electrolysis time.[13] However, in order to record a series of CV, the reaction process has to be frequently stopped. In addition, it is always difficult to calculate precisely the peak charge in the CV on account of the baseline problem. Furthermore, an electrochemical method is not applicable in evaluating the kinetics of CO coordination because anodic oxidation of the CO molecule dissolved in solution greatly affects the accuracy of the measurement of the CV of the SAM, especially in aqueous solutions. In the present study, the kinetics of the CO liberation and coordination process are analyzed from the in situ IR spectra recorded synchronously with the reactions. Compared to the electrochemical methods, this method is more efficient because it is continuous and in real-time with high time resolution and accuracy. Assuming that the IR peak intensity of the CO ligand is proportional to the amount of triruthenium complex containing CO assembled on the surface of the gold electrode, the rate constant can be estimated from the variation of the IR peak intensity of the CO ligand as a function of the reaction time.

CO liberation kinetics: The CO liberation reaction can be described by the equilibrium given in Equation (1).

$$[Ru_3^{III,III,III}-CO]^+ + solvent \underset{k_{-1}}{\overset{k_1}{\rightleftharpoons}} [Ru_3^{III,III,III}-solvent]^+ + CO \quad (1)$$

Because the CO ligand does not bind to the triruthenium cluster monolayer at $+0.90$ V in the $[Ru_3^{III,III,III}$–solvent$]^+$ state, as described above, the reverse reaction can be ignored at this potential ($k_1 \gg k_{-1} \approx 0$). In a similar manner to the previous procedure for the rate analysis of the CO liberation process,[13] a first-order rate law [Eq. (2)] can be applied to CO liberation in the SAM.

$$\ln\frac{A_0}{A} = k_1 \times t \quad (2)$$

In Equation (2), A_0 and A are the CO peak intensities at 2060 cm^{-1} initially and at time t after the start of the electrolysis at $+0.90$ V; they are proportional to the concentration of triruthenium cluster containing CO initially and at reaction time t, respectively. Figure 10 shows a plot of Equation (2) which is fitted to a linear function giving a slope of $5.4(\pm0.3)\times10^{-4}\ s^{-1}$, namely the rate constant for the CO liberation from the SAM. Unfortunately, there are no kinetic results on the homogeneous solution reaction for comparison with the SAM data in acetonitrile solution. In aqueous solution, the CO liberation rate constant of the SAM, deduced by the same method, is $1.4(\pm0.1)\times10^{-3}\ s^{-1}$, which is close to the previously reported result.[13] CO liberation was also investigated in 1,2-dicloroethane for comparison. The rate constant was evaluated to be $1.3(\pm0.1)\times10^{-3}\ s^{-1}$, which is close to the result in the aqueous solution. The details of the CO liberation rate in different solvents are given in Table 4. The reaction rate of CO liberation is dependent on

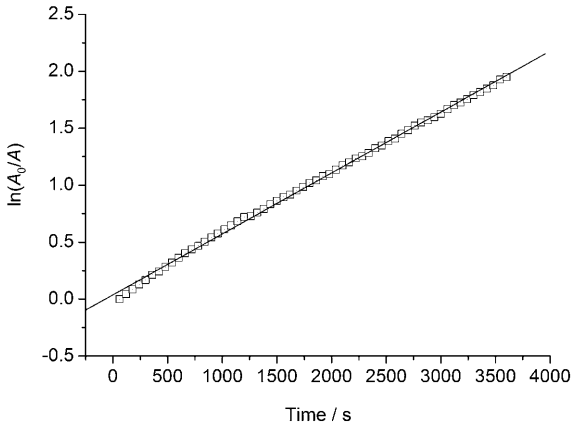

Figure 10. Rate constant of CO liberation from the SAM at room temperature (25 °C) from first-order kinetics. A_0 and A are the peak intensities of the CO peak at 2060 cm^{-1} at the initial and at time t after the start of the electrolysis, respectively.

Table 4. Rate constants for the CO liberation and recovery processes in the SAM at 25 °C in nonaqueous and aqueous solutions.

Solution	$k_{\text{CO liberation}}$ [s^{-1}]	$k_{\text{CO recovery}}$ [s^{-1}]
$HClO_4/H_2O$ (0.1 M)	$1.4(\pm0.1)\times10^{-3}$	$1.3(\pm0.1)\times10^{-3}$
$TBAPF_6/CH_3CN$ (0.1 M)	$5.4(\pm0.3)\times10^{-4}$	$1.2(\pm0.1)\times10^{-3}$
$TBAPF_6$/1,2-dichloroethane (0.1 M)	$1.3(\pm0.1)\times10^{-3}$	$1.2(\pm0.1)\times10^{-3}$

the solvent employed. The interaction between the solvent and the SAM should be an important factor. However, the exact role played by the solvent molecule in the ligand exchange reaction in the SAM is still not clear yet.

CO coordination kinetics: The CO coordination reaction in the SAM can be represented by the equilibrium given in Equation (3).

$$[Ru_3^{II,III,III} - \text{solvent}]^0 + CO \underset{k'_{1-1}}{\overset{k'}{\rightleftharpoons}} [(Ru^{II} - CO)Ru^{III}Ru^{III}]^0 + \text{solvent} \quad (3)$$

The Ru–CO bond remains intact at −0.3 V in the state $[(Ru^{II}–CO)Ru^{III}Ru^{III}]^0$, and the reverse reaction can be neglected at this potential ($k'_1 \gg k'_{-1} \approx 0$). A first-order rate law has been applied to the CO re-coordination reaction and leads to Equation (4); where A and A_f are the CO peak (1940 cm^{-1}) intensities at reaction time t and after the reaction at −0.3 V, respectively.

$$\ln\frac{A_f}{A_f - A} = k'_1 \times t \quad (4)$$

The function $\ln[A_f/(A_f - A)]$ was plotted against the reaction time t; the linear fit gives the reaction rate constant. According to Figure 11, the rate constant for CO coordination in acetonitrile solution is $1.2(\pm0.1)\times10^{-3}$ s^{-1}, which is similar to those observed in aqueous solutions ($1.3(\pm0.1)\times10^{-3}$ s^{-1}) and 1,2-dichloroethane solutions ($1.2(\pm0.1)\times10^{-3}$ s^{-1}). The solvent effect in the CO re-coordination reaction seems to be less than that observed in the CO liberation process.

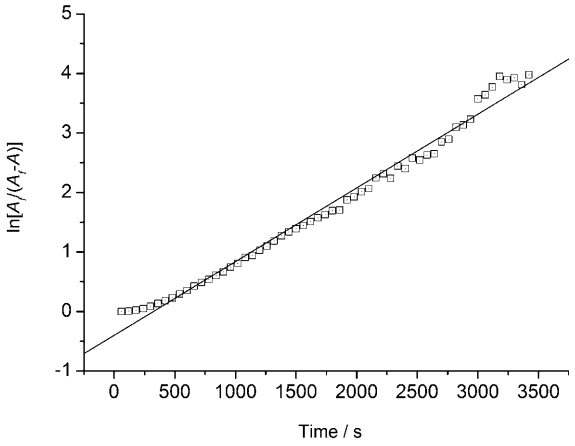

Figure 11. Rate constant of the CO ligand recovery by the solvent-SAM at room temperature (25 °C) from first-order kinetics. A_f and A are the intensity of the CO peak at 1940 cm^{-1} after a reaction time of 1 h and during reaction, respectively.

Temperature effect on CO exchange kinetics: In the reversible CO ligand exchange in the triruthenium cluster monolayer, the temperature is expected to be an important key factor. A study of the temperature effect on the CO ligand-exchange rate can provide basic kinetic information, including the reaction rates at different temperatures and the activation energy of the reaction.

The CO liberation and recovery processes were monitored in acetonitrile solution at temperatures ranging from −30 °C to +50 °C by in situ IR measurement. The normalized IR peak intensities of CO in Ru^{III}–CO during the CO liberation process and in Ru^{II}–CO during the CO recovery process at different temperatures are shown as a function of time in Figure 12a and b, respectively, at different temperatures. As the temperature decreases, both the rates of CO liberation and recovery decrease. At −30 °C, the CO liberation rate is so slow that the IR peak intensity of CO in Ru^{III}–CO is almost constant with time, implying that the CO ligand is stabilized at the Ru^{III} site at low temperatures and thus the CO ligand-exchange process almost stops at temperatures as low as −30 °C. This is an extremely interesting feature exhibited by the SAM, and time-resolved IR measurements at low temperature are being carried out in our laboratory to gain further information on the possible reaction intermediate. Conversely, an increase in the temperature leads to a high CO exchange rate as well as to desorption of the SAM from the surface of the gold electrode.

The rate constants of both the CO liberation and recovery processes at different temperatures are listed in Table 5. From the Arrhenius equation, the activation energies calculated from the slopes of the $\ln k$ versus $1/T$ plots (Figure 12c and d) are ≈53.0 kJ mol^{-1} and ≈50.0 kJ mol^{-1} for the CO liberation at +0.9 V and the recovery processes at −0.3 V, respectively. To analyze this ligand-exchange process and to understand its mechanism in detail, studies of the Arrhenius relationships of the CO-liberation and CO-coordination processes as a function of the electrode potentials are in progress in our laboratory.

Conclusion

In the present work, we have confirmed a novel CO ligand-exchange cycle in the SAM of the oxo-triruthenium cluster $[Ru_3(\mu_3\text{-}O)(\mu\text{-}CH_3COO)_6(CO)(L^1)(L^2)]$ (L^1 = $[(NC_5H_4)CH_2NHC(O)(CH_2)_{10}S\text{-}]_2$, L^2 = 4-methylpyridine) under electrochemical control. The oxidation state of the triruthenium cluster center is crucial to the ligand-exchange reactions. The CO-free SAM, that is, solvent-SAM, can be generated upon oxidation of the SAM to the state $[Ru_3^{III,III,III}–CO]^+$, while solvent-SAM can be returned to CO-SAM when it is electrochemically reduced to the

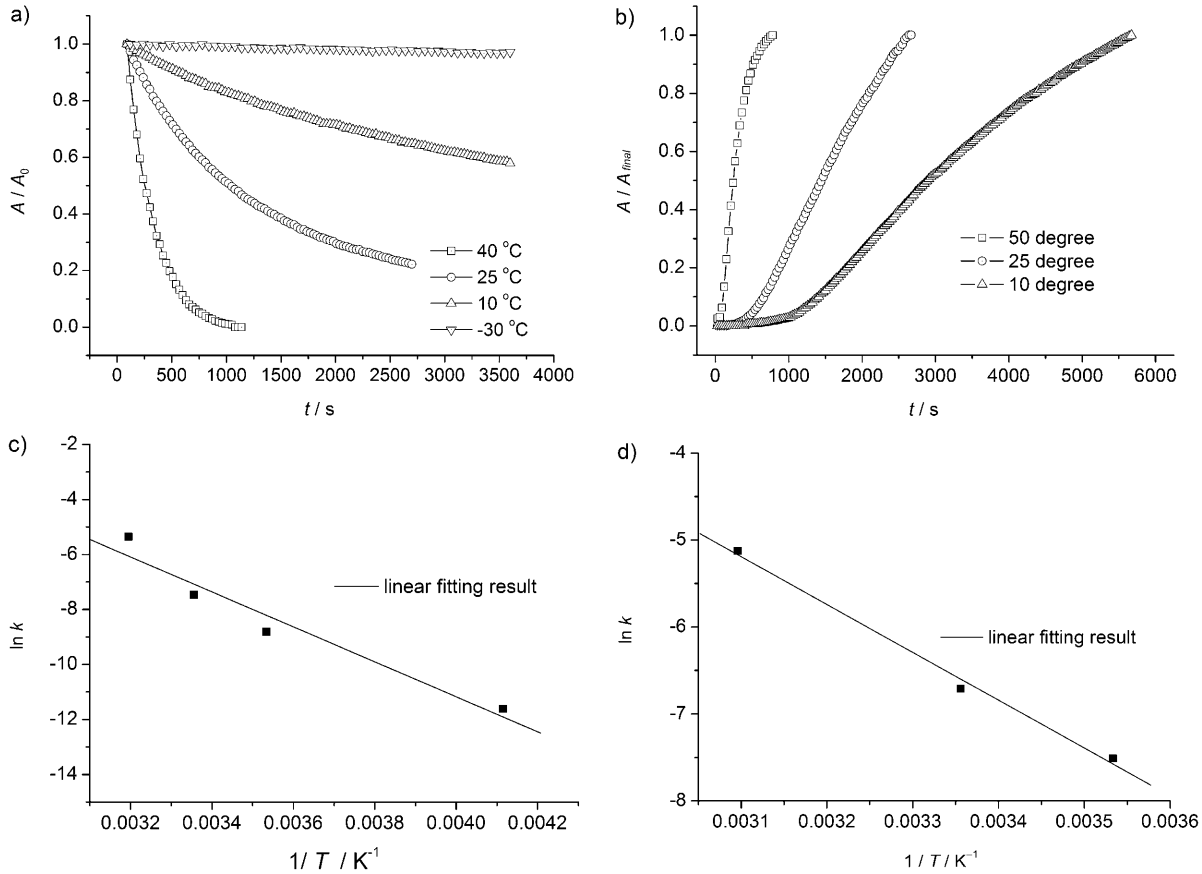

Figure 12. a and b: Plots of normalized IR intensity of the CO peak at different temperatures versus the reaction time in the CO liberation and recovery processes in $TBAPF_6/CH_3CN$ (0.1 M), respectively. Integration time for each spectrum is 30 s. c and d: Plots of $\ln k$ versus $1/T$ of the CO liberation and recovery processes, respectively.

Table 5. Reaction rate constants for CO liberation and recovery in the SAM at various temperatures in $TBAPF_6/CH_3CN$ (0.1 M) solution.

T[°C]	$k_{CO\ liberation}$[s^{-1}]	$k_{CO\ recovery}$[s^{-1}]
50	–	5.8×10^{-3}
40	4.8×10^{-3}	–
25	5.4×10^{-4}	1.2×10^{-3}
10	1.5×10^{-4}	4.5×10^{-4}
−30	9.0×10^{-6}	–

$[Ru_3^{II,III,III}$–solvent$]^0$ state in contact with CO in solution. The CO exchange process is greatly affected by the temperature and can be nearly stopped at low temperature, which provides a useful tuning factor for CO switching control. Kinetics of both the CO liberation and coordination of the triruthenium cluster on the electrode surface were evaluated by in situ IR spectroscopy.

The reversible ligand-exchange capability of the metal cluster nanostructure on the electrode surface is of great interest for the future development of a novel CO molecule recognition nanodevice. Electrochemically triggered NO ligand exchange in a SAM containing a triruthenium cluster was also achieved recently and will be reported in a later paper.

Experimental Section

The synthesis of the triruthenium complex has been described elsewhere.[13] An approximately 50 nm-thick gold film, which was chemically deposited on the reflecting surface of a hemicylindrical Si prism with a dimension of 2.5×2 cm^2,[58] was used as a substrate for monolayer construction and also served as the working electrode. The roughness factor of the gold film surface was estimated to be 4.0 from the reduction charge of gold oxide on the cyclic voltammogram of the gold film between 0.0 and +1.6 V versus SCE (all potentials in this paper are referenced to SCE) at a scan rate of 1 V s^{-1}. After the gold electrode surface was electrochemically cleaned by sweeping the electrode potential between 0.0 V and +1.4 V for 2–5 cycles, the gold substrate was immersed in an ethanol solution of the complex (50 μM) for about 20 h at room temperature to construct the SAM of the triruthenium complex. The modified gold electrode was rinsed with copious quantities of ethanol, dried with Ar gas, and finally mounted in an spectroelectrochemical cell for electrochemical and in situ IR spectroscopic measurements. A sample of the SAM for ex situ IR reflection absorption spectroscopic (IRRAS) measurement was prepared on a gold film (ca. 200 nm thick) evaporated on a Ti-coated (ca. 2 nm thick) glass plate.

The reaction process was monitored by means of in situ IR measurement with the Kretschmann attenuated total reflection (ATR) configuration.[59] The use of an ATR configuration for IR measurement facilitates the in situ monitoring of the electrode process owing to the fact that it is free from the mass transport problem. This problem is inherent in conventional in situ IR reflection absorption spectroscopy in which a thin solution layer is needed between the reflective electrode surface and the IR window.[60] IR spectra at 4 cm^{-1} resolution were recorded on a Bio-Rad

FTS 60 A/896 FT-IR spectrometer equipped with a liquid nitrogen-cooled MCT detector. All the IR spectra are shown in absorbance units, defined as $A = -\log I/I_0$, where I and I_0 represent the IR absorption intensities of the sample state and background state, respectively. The integration time of the IR spectra in different experiments ranged from 3 s to 60 s, and are given in the Figure captions. A homemade single-reflection accessory (incident angle of 70°) and a Harrick grazing angle (ca. 70°) reflection accessory were used for in situ and ex situ IR measurements, respectively. The spectroelectrochemical cells were of a three-electrode design.[61]

In situ sum-frequency generation (SFG) measurement in a thin-layer cell was also employed to characterize the SAM. The SFG spectra were recorded with a broad-band femtosecond SFG system constructed by our group. Details of the system have been described elsewhere.[62–64]

The counter electrode was a Pt foil and the reference electrode was either a saturated calomel electrode (SCE) for aqueous solutions or a Ag/Ag^+ electrode for organic electrolyte solutions. Aqueous solutions of 0.1 M $HClO_4$ and nonaqueous solutions of CH_3CN or 1,2-dichloroethane with nBu$_4$NPF$_6$ (TBAPF$_6$, 0.1 M) were employed as the electrolytes. A potentiostat (model 263 A, EG&G PARC) was used to control the electrode potential. Prior to electrochemical measurement, the electrolyte solution was deaerated with Ar gas for about 30 min.

In temperature-controlled experiments, a homemade double-jacketed spectroelectrochemical cell and a programmable low-temperature bath (model NCB-1200, Rikakikai, Tokyo), with which the temperature was controlled in the range between −30 °C and 95 °C.

All reagents and solvents were of commercially available analytical-grade quality, unless otherwise stated. The CO gas was of ultra-high purity (Sumitomo Seika, Japan).

Acknowledgements

Y.S. gratefully acknowledges the support from PRESTO, Japan Science and Technology Corporation (JST). Y.S. also acknowledges the support from the SHISEIDO Fund for Science and Technology, 2001 Corning Research Grants, and Akiyama Foundation.

[1] Special Issue: Supramolecular Chemistry and Self-Assembly, *Science* **2002**, *295*, 2395.
[2] Special Issue on "Organic-Inorganic Nanocomposite Materials", *Chem. Mater.* **2001**, *13*, 3059.
[3] V. Balzani, M. Venturi, A. Credi, *Molecular Devices and Machines: A Journey into the Nanoworld*, Wiley-VCH, Weinheim; Cambridge, **2003**.
[4] A. Ulman, *An Introduction to Ultra-Thin Organic Films from Langmuir-Blodgett to Self-Assembly*, Academic Press, San Diego, CA, **1991**.
[5] A. Ulman, *Chem. Rev.* **1996**, *96*, 1533.
[6] F. Schreiber, *Prog. Surf. Sci.* **2000**, *65*, 151.
[7] J. Xu, H.-L. Li, *J. Colloid Interface Sci.* **1995**, *176*, 138.
[8] A. N. Shipway, E. Katz, I. Willner, *ChemPhysChem* **2000**, *1*, 18.
[9] I. Willner, E. Katz, *Angew. Chem.* **2000**, *112*, 1230; *Angew. Chem. Int. Ed.* **2000**, *39*, 1180.
[10] R. K. Smith, P. A. Lewis, P. S. Weiss, *Prog. Surf. Sci.* **2004**, *75*, 1.
[11] J. H. Fendler, *Chem. Mater.* **2001**, *13*, 3196.
[12] B. F. G. Johnson, *Coord. Chem. Rev.* **1999**, *190–192*, 1269.
[13] A. Sato, M. Abe, T. Inomata, T. Kondo, S. Ye, K. Uosaki, Y. Sasaki, *Phys. Chem. Chem. Phys.* **2001**, *3*, 3420.
[14] M. Abe, T. Michi, A. Sato, T. Kondo, W. Zhou, S. Ye, K. Uosaki, Y. Sasaki, *Angew. Chem.* **2003**, *115*, 3018; *Angew. Chem. Int. Ed.* **2003**, *42*, 2912.
[15] C. Lin, C. R. Kagan, *J. Am. Chem. Soc.* **2003**, *125*, 336.
[16] S. Sortino, S. Petralia, S. Conoci, S. D. Bella, *J. Am. Chem. Soc.* **2003**, *125*, 1122.
[17] F. A. Cotton, J. G. Norman, *Inorg. Chim. Acta* **1972**, *6*, 411.
[18] A. Spencer, G. Wilkinson, *J. Chem. Soc. Dalton Trans.* **1972**, 1570.
[19] A. Spencer, G. Wilkinson, *J. Chem. Soc. Dalton Trans.* **1974**, 786.
[20] S. T. Wilson, R. F. Bondurant, T. J. Meyer, D. J. Salmon, *J. Am. Chem. Soc.* **1975**, *97*, 2285.
[21] J. A. Baumann, D. J. Salmon, S. T. Wilson, T. J. Meyer, W. E. Hatfield, *Inorg. Chem.* **1978**, *17*, 3342.
[22] J. A. Baumann, D. J. Salmon, S. T. Wilson, T. J. Meyer, W. E. Hatfield, *Inorg. Chem.* **1979**, *18*, 2472.
[23] R. D. Cannon, R. P. White, *Prog. Inorg. Chem.* **1988**, *36*, 195.
[24] T. Ito, T. Hamaguchi, H. Nagino, T. Yamaguchi, J. Washington, C. P. Kubiak, *Science* **1997**, *277*, 660.
[25] K. Ota, H. Sasaki, T. Matsui, T. Hamaguchi, T. Yamaguchi, T. Ito, H. Kido, C. P. Kubiak, *Inorg. Chem.* **1999**, *38*, 4070.
[26] H. E. Toma, K. Araki, A. D. P. Alexiou, S. Nikolaou, S. Dovidauskas, *Coord. Chem. Rev.* **2001**, *219*, 187.
[27] J.-L. Chen, L.-Y. Zhang, Z.-N. Chen, L.-B. Gao, M. Abe, Y. Sasaki, *Inorg. Chem.* **2004**, *43*, 1481.
[28] S. Ye, W. Zhou, M. Abe, T. Nishida, L. F. Cui, K. Uosaki, M. Osawa, Y. Sasaki, *J. Am. Chem. Soc.* **2004**, *126*, 7434.
[29] M. Abe, Y. Sasaki, Y. Yamada, K. Tsukahara, S. Yano, T. Yamaguchi, M. Tominaga, I. Taniguchi, T. Ito, *Inorg. Chem.* **1996**, *35*, 6724.
[30] M. Claybourn, in *Handbook of Vibrational Spectroscopy, Vol. 2* (Eds.: J. M. Chalmers, P. R. Griffiths), Wiley, Chichester (UK), **2002**, pp. 969.
[31] M. K. Johnson, D. B. Powell, R. D. Cannon, *Spectrochim. Acta* **1981**, *37*, 995.
[32] A. Ohto, A. Tokiwa-Yamamoto, M. Abe, T. Ito, Y. Sasaki, K. Umakoshi, R. D. Cannon, *Chem. Lett.* **1995**, 97.
[33] H. E. Toma, C. Cipriano, *J. Electroanal. Chem.* **1989**, *263*, 313.
[34] M. Abe, A. Sato, T. Inomata, T. Kondo, K. Uosaki, Y. Sasaki, *J. Chem. Soc. Dalton Trans.* **2000**, 2693.
[35] S. Ye, H. Akutagawa, K. Uosaki, Y. Sasaki, *Inorg. Chem.* **1995**, *34*, 4527.
[36] C. A. Widrig, C. Chung, M. D. Porter, *J. Electroanal. Chem.* **1991**, *310*, 335.
[37] T. W. Schneider, D. A. Buttry, *J. Am. Chem. Soc.* **1993**, *115*, 12391.
[38] Y.-J. Cho, H. Song, K. Lee, K. Kim, J. Kwak, S. Kim, J. T. Park, *Chem. Commun.* **2002**, 2966.
[39] H. Imahori, *J. Phys. Chem. B* **2004**, *108*, 6130.
[40] Z. Liu, A. A. Yasseri, J. S. Lindsey, D. F. Bocian, *Science* **2003**, *302*, 1543.
[41] M. Abe, Y. Sasaki, A. Nagasawa, T. Ito, *Bull. Chem. Soc. Jpn.* **1992**, *65*, 1411.
[42] Y. Sato, S. Ye, T. Haba, K. Uosaki, *Langmuir* **1996**, *12*, 2726.
[43] K. Shimazu, S. Ye, Y. Sato, K. Uosaki, *J. Electroanal. Chem.* **1994**, *375*, 409.
[44] S. Ye, A. Yashiro, Y. Sato, K. Uosaki, *J. Chem. Soc. Faraday Trans.* **1996**, *92*, 3813.
[45] S. Ye, Y. Sato, K. Uosaki, *Langmuir* **1997**, *13*, 3157.
[46] A. D. E. Pullin, *Spectrochim. Acta* **1958**, *13*, 125.
[47] L. B. Archibald, A. D. E. Pullin, *Spectrochim. Acta* **1958**, *12*, 34.
[48] J.-L. Rivail, D. Rinaldi, V. Diliet, *Mol. Phys.* **1996**, *89*, 1521.
[49] Y. R. Shen, *The Principles of Nonlinear Optics*, Wiley, Inc, New York, **1984**.
[50] C. D. Bain, *J. Chem. Soc. Faraday Trans.* **1995**, *91*, 1281.
[51] M. Buck, M. Himmelhaus, *J. Vac. Sci. Technol.* **2001**, *19*, 2717.
[52] R. E. Kitson, N. E. Griffith, *Anal. Chem.* **1952**, *24*, 334
[53] H. W. Thompson, G. Steel, *Trans. Faraday Soc.* **1956**, *52*, 1451.
[54] I. S. Zavarine, C. P. Kubiak, T. Yamaguchi, K.-i. Ota, T. Matsui, T. Ito, *Inorg. Chem.* **2000**, *39*, 2696.
[55] G. Powell, D. T. Richens, A. K. Powell, *Inorg. Chim. Acta* **1993**, *213*, 147.
[56] Y. Sasaki, A. Nagasawa, A. Tokiwa-Yamamoto, T. Ito, *Inorg. Chim. Acta* **1993**, *212*, 175.
[57] Y. Sasaki, K. Umakoshi, T. Imamura, A. Kikuchi, A. Kishimoto, *Pure Appl. Chem.* **1997**, *69*, 205.
[58] H. Miyake, S. Ye, M. Osawa, *Electrochem. Commun.* **2002**, *4*, 973.

[59] M. Osawa, in *Handbook of Vibrational Spectroscopy*, *Vol. 1* (Eds.: J. M. Chalmers, P. R. Griffiths), Wiley, Chichester (UK), **2002**, pp. 785.
[60] T. Iwasita, F. C. Nart, *Prog. Surf. Sci.* **1997**, *55*, 271.
[61] K. Ataka, T. Yotsuyanagi, M. Osawa, *J. Phys. Chem.* **1996**, *100*, 10664.
[62] S. Ye, H. Noda, S. Morita, K. Uosaki, M. Osawa, *Langmuir* **2003**, *19*, 2238.
[63] S. Ye, H. Noda, T. Nishida, S. Morita, M. Osawa, *Langmuir* **2004**, *20*, 357.
[64] J. Holman, S. Ye, D. J. Neivandt, P. B. Davies, *J. Am. Chem. Soc.* **2004**, *126*, 14322.

Received: December 27, 2004
Published online: June 24, 2005